

## Microscopic Coupled-channels Studies of $\alpha$ cluster structures in $^{19}\text{Ne}$

---

Reiji Otani, Masataka Iwasaki, Makoto Ito\*

*Department of Pure and Applied Physics, Kansai University*

*E-mail: itomk@kansai-u.ac.jp*

Cluster structures in  $^{19}\text{Ne}$  are studied by the microscopic cluster model, the generalized two-center cluster model (GTCM). In the GTCM calculation, the coupled-channels problem of  $(^3\text{He}+^{16}\text{O}) + (\alpha+^{15}\text{O})$  is solved, and the adiabatic energy surfaces, which are the series of the energy eigenvalues as a function of the He–O distance, are investigated. In the adiabatic energy curves, the several local minima are generated in the spatial region of the small core distance, where the neutron hole inside of the He or O nucleus is strongly coupled to the residual nuclei. The energy spectra, which are constructed from the strong coupling states, nicely reproduce the the low-lying energy levels in the  $^{19}\text{Ne}$  nucleus. The extended microscopic calculations of  $(^3\text{He}+^{16}\text{O}) + (\alpha+^{15}\text{O}) + (^5\text{He}+^{14}\text{O})$  are performed in order to see the coupling effect of the  $5p-2h$  configuration, which corresponds to the shell model limit of the  $^5\text{He} + ^{14}\text{O}$  cluster configuration. The extended calculation suggests that the  $^5\text{He} + ^{14}\text{O}$  configuration plays an important role on the formation of the  $3/2^+$  resonance at 0.5 MeV with respect to the  $\alpha$  threshold.

*The 26th International Nuclear Physics Conference  
11-16 September, 2016  
Adelaide, Australia*

---

\*Speaker.

## 1. Introduction

The  $\alpha$  cluster structures have been extensively studied for the so-called  $4N$  nuclei with  $N = Z$ , such as  $^8\text{Be} = 2\alpha$ ,  $^{12}\text{C} = 3\alpha$ ,  $^{16}\text{O} = \alpha + ^{12}\text{C}$ , and  $^{20}\text{Ne} = \alpha + ^{16}\text{O}$  [1, 2, 3]. In current studies, the importance of the cluster degrees of freedom has been extended to the neutron-rich ( $N > Z$ ) systems, which are obtained by adding extra neutrons to the  $4N$  cluster systems. In the neutron-rich systems, such as  $^{12}\text{Be} = 2\alpha + 4N$  [4],  $^{16}\text{C} = 3\alpha + 4N$  [5] and  $^{22}\text{Ne} = \alpha + ^{16}\text{O} + 2N$  [6], various chemical-bonding-like structures are generated by the coupling of the cluster relative motion and the single particle motion of extra neutrons. In particular, the drastic structure changes among the chemical bonding-like states are pointed out in the continuum energy region of  $^{12}\text{Be}$  [4].

On the contrary, cluster structures in the  $4N$  systems with a hole in a cluster core, are also interesting research subjects [7, 8, 9, 10, 11]. For example, there is a recent study of  $^{11}\text{B} = \alpha + \alpha + t$ , corresponding to a proton hole system of  $^{12}\text{C} = 3\alpha$  [7]. Pioneering work of the hole system is the study of the  $^{19}\text{F}$  nucleus [8, 9, 11, 10]. The  $^{19}\text{F}$  nucleus is the one proton deficient system of  $^{20}\text{Ne}$ , and the rotational bands of  $\alpha + ^{15}\text{N}$  and  $t + ^{16}\text{O}$ , which are calculated from the folding type potential, were clearly assigned to the energy levels observed in the  $\alpha$  and  $t$  transfer reactions [8]. The energy levels in  $^{19}\text{F}$  have also been analyzed in the more sophisticated models, such as the full microscopic  $\alpha + ^{15}\text{N}$  cluster model on the basis of the generator coordinate method (GCM) [9, 11] and the orthogonalized condition model (OCM) of the  $(t + ^{16}\text{O}) + (\alpha + ^{15}\text{N})$  coupled-channels [10]. In the coupled-channels analysis,  $t$  and  $\alpha$  cluster bands are clearly identified although a considerable mixture of these two configurations occurs.

In the previous analyses on  $^{19}\text{F}$  [9, 10], the so-called weak coupling states of the proton hole and the cluster relative motion are confirmed above the  $\alpha$  threshold energy. For example, in the  $\alpha + ^{15}\text{N}$  system, a proton hole inside of the  $^{16}\text{O}$  cores loosely couples to the relative motion of the  $\alpha + ^{16}\text{O}$  cluster cores. In a naive consideration, the weak coupling state of the hole in  $^{16}\text{O}$  and the  $\alpha$  particle is also expected in the neutron-deficient system,  $\alpha + ^{15}\text{O}$  in  $^{19}\text{Ne}$  [11, 10]. In fact, a formation of  $\alpha + ^{15}\text{O}$  in  $^{19}\text{Ne}$  was discussed from the perspective of  $^{19}\text{F} - ^{19}\text{Ne}$  Coulomb displacement energy [8, 10]. However, detailed analysis of the energy levels over a wide energy region, which covers the unbound continuum states, such as the analysis of the resonance width above the  $\alpha$  threshold and the excitation function of the resonant scattering, have not been undertaken yet because available experimental data are still limited. Therefore, a study of the  $\alpha + ^{15}\text{O}$  cluster structure in  $^{19}\text{Ne}$ , corresponding to the  $N < Z$  system, is very interesting from the viewpoint of the systematics of the clustering phenomena in the  $N \neq Z$  systems.

Recently, we have applied the potential model to the  $\alpha + ^{15}\text{O}$  system [12] and predicted the existence of the resonances, which have the weak coupling feature, above the  $\alpha$  threshold. The potential model is useful to understand the resonant states, in which the  $\alpha$  clustering is well developed. However, the microscopic cluster model, in which the anti-symmetrization among the nucleons are completely performed, is very important in analyzing the energy levels from the low-lying states to the highly-excited states in a unified manner. In particular, the anti-symmetrization effect is essential for the low-lying states, which is difficult to handle in the potential model. In the present report, we apply the microscopic cluster model of  $(^3\text{He} + ^{16}\text{O}) + (\alpha + ^{15}\text{O})$  and analyze the low-lying and highly resonant states in  $^{19}\text{Ne}$  [12].

There is another reason why we focus on the  $\alpha + ^{15}\text{O}$  structure in the  $^{19}\text{Ne}$  nucleus. The

$^{15}\text{O}(\alpha, \gamma)^{19}\text{Ne}$  reaction is known to play a crucial role in the advanced stages of astrophysical hydrogen burning [14]. In the  $^{15}\text{O}(\alpha, \gamma)^{19}\text{Ne}$  reaction, the most crucial resonance is known to arise through the  $J^\pi = 3/2^+$  resonant level at 504 keV with respect to the  $\alpha + ^{15}\text{O}$  threshold ( $E_x = 4.03$  MeV). Unfortunately, direct measurement of the resonance at 504 keV is still difficult because of the small strength of the resonance and its energy position extremely close to the  $\alpha$  decay threshold. The analyses in Ref. [15] have pointed out that the intrinsic structure of the resonance at 504 keV in  $^{19}\text{Ne}$  is not the  $\alpha + ^{15}\text{O}$  cluster structure, but the five particle–two hole ( $5p-2h$ ) shell-model configuration with the  $^{14}\text{O}_{g.s.}$  core. The  $5p-2h$  configuration has a large overlap with the shell model limit of the  $^5\text{He} + ^{14}\text{O}$  configuration. Therefore, the coupling of  $^5\text{He} + ^{14}\text{O}$  on the  $J^\pi = 3/2^+$  state is essential in the cluster model approach. In this report, the result of the extended microscopic calculation of  $(^3\text{He} + ^{16}\text{O}) + (\alpha + ^{15}\text{O}) + (^5\text{He} + ^{16}\text{O})$  in  $J^\pi = 3/2^+$  will also be reported.

## 2. Framework

### 2.1 microscopic cluster model

We apply the generalized two-center cluster model (GTCM) for the calculations of the low-lying levels [4]. The GTCM is the extended model of the microscopic cluster model on the basis of the generator coordinate method (GCM) [16]. The application of GTCM to Be isotopes ( $\alpha + \alpha + N + N + \dots$ ) has already been published in Ref. [4], and we briefly explain the formulation of GTCM in the  $^{19}\text{Ne}$  nucleus. The basis function for  $^{19}\text{Ne}$  is given by

$$\Phi_{\mathbf{m}}^{J^\pi K}(S) = \hat{P}_K^{J^\pi} \mathcal{A} \left\{ \psi(^3\text{He}) \psi(^{14}\text{O}) \prod_{j=1}^2 \varphi_j(m_j) \right\}_S. \quad (2.1)$$

The basis function is constructed on the basis of  $^3\text{He} + ^{14}\text{O}$  cores, and the two neutrons are treated as the active valence-nucleons. The  $\psi(^3\text{He})$  and  $\psi(^{14}\text{O})$  represent the core wave functions of the  $^3\text{He}$  and  $^{14}\text{O}$  nuclei, respectively. The former part is described by the  $(0s)^3$  configuration in the harmonic oscillator (HO) potential, while the latter part is constructed by the  $(0s)^4(0p)^{10}$  configuration. Two centers are placed with the relative distance parameter  $S$ , which is treated as the generator coordinate. The single-particle wave function for the  $j$ -th valence neutrons ( $j = 1, 2$ ) localized around the  $^3\text{He}$  or  $^{14}\text{O}$  clusters is given by an atomic orbital (AO)  $\varphi(m_j)$ , which is classified by a set of the AO quanta of  $m_j = (k, C, \tau)$  with the HO orbitals  $k$ , the core  $C$ , and the neutron spin  $\tau$  ( $= \uparrow$  or  $\downarrow$ ). The HO orbitals around the core  $C$  ( $C = ^3\text{He}$  or  $^{14}\text{O}$ ) are  $k = 0s$  ( $C = ^3\text{He}$ ) or  $k = 0p$  ( $C = ^{14}\text{O}$ ). The basis functions with the AO quanta of two valence neutrons,  $\mathbf{m} = (m_1, m_2)$ , are fully anti-symmetrized by the anti-symmetrizer  $\mathcal{A}$  and projected to the eigenstate of the total spin  $J$ , its intrinsic angular projection  $K$ , and the total parity  $\pi$  by the projection operator  $\hat{P}_K^{J^\pi}$ .

The total wave function is finally given by taking the superposition over  $S$ ,  $\mathbf{m}$  and  $K$  as

$$\hat{\Psi}_v^{J^\pi} = \int dS \sum_{\mathbf{m}, K} C_{\mathbf{m}K}^{J^\pi v}(S) \Phi_{\mathbf{m}}^{J^\pi K}(S). \quad (2.2)$$

The coefficients  $C_{\mathbf{m}K}^{J^\pi v}(S)$  in Eq. (2.2) for the  $v$ -th eigenstate are determined by solving a coupled channel GCM (Generator Coordinate Method) equation [16]

$$\left\langle \Phi_{\mathbf{m}}^{J^\pi}(S) \left| \hat{H} - E_v^{J^\pi} \right| \Psi_v^{J^\pi} \right\rangle = 0. \quad (2.3)$$

Here  $\hat{H}$  and  $E_\nu^{J^\pi}$  denote the total Hamiltonian and the energy eigenvalues of the  $\nu$ -th eigenstate for the  $J^\pi$  state, respectively. Before solving Eq. (2.3), we can investigate the structure changes with respect to the variation of the  $^3\text{He}$ - $^{14}\text{O}$  distance parameter. Namely, we solve the eigenvalue problem at a fixed  $S$ , such as

$$(\hat{H} - E_\mu^{J^\pi}(S)) \Phi_{AS}^{J^\pi\mu}(S) = 0 \quad (2.4)$$

with

$$\Phi_{AS}^{J^\pi\mu}(S) = \sum_{\mathbf{mK}} D_{\mathbf{mK}}^{J^\pi\mu}(S) \Phi_{\mathbf{mK}}^{J^\pi\mu}(S) . \quad (2.5)$$

The  $\mu$ -th eigenvalue  $E_\mu^{J^\pi}(S)$  is a function of the relative distance-parameter  $S$ , and a sequence of  $E_\mu^{J^\pi}(S)$  forms the energy surfaces. The energies  $E_\mu^{J^\pi}(S)$  and wave functions  $\Phi_{AS}^{J^\pi\mu}(S)$  correspond to the so-called ‘‘adiabatic energy surfaces (AESs)’’ and ‘‘adiabatic states (ASs)’’, respectively, in atomic physics [4]. The detailed properties of AESs and ASs are reported in Ref. [4].

As for the nucleon-nucleon (NN) interaction, we use the Volkov No.2 [17] and the G3RS [18] for the central and spin-orbit parts, respectively. The parameters in the NN interactions and the size parameter of HO are tuned to reproduce the  $^3\text{He}$  and  $^4\text{He}$  decay threshold of  $^{19}\text{Ne}$  as much as possible. In the present calculation, the HO size parameter is set to  $b = 1.6$  fm, while the strength of the Volkov No. 2 are taken to be  $\pm 60$  MeV without Bartlett and Heisenberg terms ( $B = H = 0$ ). This parameter setting is the same as the previous microscopic calculation in  $^{19}\text{F}$  [11]. We have found that the strength of Majorana term ( $M$ ) must be varied depending on the parity:  $M = 0.638$  for the positive parity and  $M = 0.62$  for the negative parity. The feature of the parity dependence is also similar to the previous study of  $^{19}\text{F}$  in Ref. [11]. The strength of the G3RS is taken to be  $\pm 1500$  MeV, which is the same order of the magnitude as the analysis of Be isotopes [4].

### 3. Results

#### 3.1 Adiabatic energy curves

Before doing the complete calculations, we solve Eq. (2.5) for the coupled channels of ( $^3\text{He}+^{16}\text{O}$ ) + ( $\alpha+^{15}\text{O}$ ) and calculate the adiabatic energy surfaces (AESs). In the AESs, the structure change from the two-body weak-coupling states to the one-body strong-coupling states occurs as the distance parameter  $S$  gets smaller [13]. The boundary of the weak and strong coupling states is  $S = 6.5$  fm, and we call this boundary distance  $S_C$ .

At the outside region of  $S_C$ , the He and O nuclei slip to each other with the internal spins ( $1/2^-$  or  $3/2^-$  for  $^{15}\text{O}$  and  $1/2^+$  for  $^3\text{He}$ ) and the relative spin of  $L$ . In the particle-hole picture, the neutron hole in  $^{16}\text{O}$  ( $\alpha$ ) weakly couples to the residual nucleus,  $\alpha$  ( $^{16}\text{O}$ ). On the contrary, in the small distance of  $S_C \leq 6.5$  fm, the effect of the nuclear interaction begins to be strong. The effect of the nuclear interaction leads to the strong mixture of the weak coupling states. The mixture of the weak coupling states corresponds the so-called strong coupling states, in which neutron holes are difficult to move inside of a nucleus freely, and the holes tend to be fixed to a certain spatial direction.

In the region of the strong coupling scheme, the local minima appear in the individual energy curves. This means that the energy levels respective to the energy minima are generated when we solve the coupled-channel GCM equation (2.3). In the present GCM calculation, the range of the

distance parameter is set to  $S = 2 \sim 5.2$  fm, which covers the local minima in the strong coupling region. Therefore, the main components of the resultant energy levels are the strong coupling states, in which the neutron holes are tightly bound around the residual nuclei. Thus, the weak coupling states are excluded in the present computational space.

The weak coupling states are also possible to appear in the energy levels if the range of the distance parameter is extended in the GCM calculation. However, the weak coupling states are mainly appear as the resonant states in the continuum energy region and hence, the consideration of the scattering boundary condition is important in the careful analysis of the weak coupling states. The analysis of the the weak coupling states under the scattering boundary condition is a future subject [4].

### 3.2 Energy spectra

In Fig. 1, the energy spectra for the positive parity states are plotted. The microscopic GCM spectra of the  $(^3\text{He}+^{16}\text{O}) + (\alpha+^{15}\text{O})$  at the right position are compared with the experimental data plotted at the left side. The GCM calculation reproduce the level ordering of the low-lying experimental spectra below the  $\alpha$  threshold (dashed line). Furthermore, the GCM calculation predict the several resonant states around  $E \geq 4$  MeV above the  $\alpha$  threshold. Therefore, it is strongly desired to identify these resonant levels experimentally.

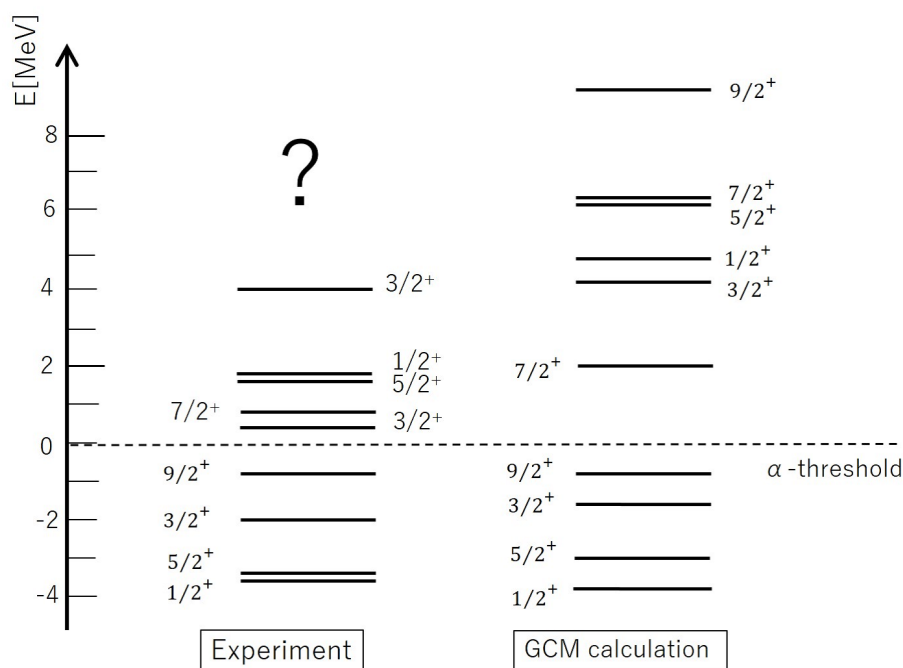


**Figure 1:** Energy levels of the positive parity states in  $^{19}\text{Ne}$ . The left levels are the experimental data, while right levels are the results of the microscopic GCM calculation with the  $(^3\text{He} + ^{15}\text{O}) + (\alpha + ^{15}\text{O})$  partitions. The dotted line represents the  $\alpha$  threshold energy, which is set to the zero energy.

On the contrary, the GCM calculation fails to reproduce a group of the resonant levels, which exists just above the  $\alpha$  threshold, such as  $3/2^+$ ,  $7/2^+$  and  $5/2^+$ . The level spacing of the present

calculation consistent to the previous studies of the coupled-channels of  $^{19}\text{F} = (t + ^{16}\text{O}) + (\alpha + ^{15}\text{N})$  [10]. In the model space of  $(^3\text{He} + ^{16}\text{O}) + (\alpha + ^{15}\text{O})$ , we have found that a group of resonances around the  $\alpha$  threshold are difficult to reproduce although several parameter sets are tested carefully. Thus, we speculate that the threshold resonances are described by the extended model space beyond the  $\alpha$  and  $^3\text{He}$  clusters. The formation of  $3/2^+$  will be discussed in the later section.

### 3.3 Effect of the $^5\text{He} + ^{14}\text{O}$ configuration

In the result shown in Fig. 1, we can confirm that the  $3/2^+$  state just above the  $\alpha$  threshold is missing in the calculations of  $(^3\text{He} + ^{16}\text{O}) + (\alpha + ^{16}\text{O})$ . This failure is the same as the results of the previous microscopic GCM calculation of  $^{19}\text{F} = \alpha + ^{15}\text{N}$  [11] and the coupled-channel OCM calculation in  $^{19}\text{F} = (^3\text{He} + ^{16}\text{O}) + (\alpha + ^{15}\text{N})$  [10]. Therefore, the  $\alpha$  and  $^3\text{He}$  cluster configurations are considered to be minor component in the threshold  $3/2^+$  state. This result is consistent to the previous experimental result, which points out the dominance of the  $5p-2h$  configuration in the threshold  $3/2^+$  state [15], because the  $\alpha + ^{15}\text{O}$  and  $^3\text{He} + ^{16}\text{O}$  cluster configurations have the large overlap with the  $4p-1h$  and  $3p-0h$  shell model configurations, respectively, in the  $S = 0$  limit.

Therefore, we should include other cluster configuration, which has a large overlap of the  $5p-2h$  state. From the viewpoint of the cluster model, the  $^5\text{He} + ^{14}\text{O}$  partition has the large overlap with the  $5p-2h$  configuration in the shell model limit ( $S \rightarrow 0$ ). In the shell model limit, the  $^5\text{He} + ^{14}\text{O}$  partition is possible to have a large overlap with the  $4p-1h$ , and  $3p-0h$  configuration as well as  $5p-2h$ . The  $4p-1h$  states, which corresponds to the negative parity states, can be projected out by the parity projection operator, while the  $3p-0h$  states can be excluded by the orthogonality condition to the  $^3\text{He} + ^{16}\text{O}$  partition, which corresponds to  $3p-0h$  configuration. Therefore, only the  $5p-2h$  configuration will be effective in the extended calculation of  $(^3\text{He} + ^{16}\text{O}) + (\alpha + ^{16}\text{O}) + (^5\text{He} + ^{14}\text{O})$  in the shell model limit.

In order to see the effect of the  $5p-2h$  configuration more directly, we have performed the  $(^3\text{He} + ^{16}\text{O}) + (\alpha + ^{16}\text{O}) + (^5\text{He} + ^{14}\text{O})$  coupled-channels for the  $3/2^+$  state. In this extended calculation, the range of the distance parameters are extended up to about 50 fm, and the resonant levels above the  $\alpha$  threshold are identified by imposing the absorbing boundary condition [20]. Thus, both the weak-coupling and strong-coupling schemes are completely taken into account.

The energy spectra are shown in Fig. 2. In the calculation of  $(^3\text{He} + ^{16}\text{O}) + (\alpha + ^{16}\text{O})$  (middle levels), there is only a bound  $3/2^+$  state around the  $\alpha$  threshold (dashed line), and no resonance appears around the threshold. On the contrary, a new levels with a dominant component of  $^5\text{He} + ^{14}\text{O}$  appear around  $E_x \sim 12$  MeV (thick level) in the extended calculation with the three partitions (right levels). However, the energy of the  $^5\text{He} + ^{14}\text{O}$  configuration is higher by about 10 MeV than the experimental  $3/2^+$  state around the  $\alpha$  threshold. The reason why the energy of the  $^5\text{He} + ^{14}\text{O}$  channel is too high is the incorrect reproduction of the threshold energy of the  $^5\text{He} + ^{14}\text{O}$  channel in the theoretical calculation. The theoretical  $^5\text{He}$  threshold is higher by about 7 MeV than the experimental threshold in the present setting of the nucleon-nucleon interaction. The  $^5\text{He}$  nucleus is unbound with respect to the  $\alpha + N$  threshold but this nucleus is handled by the simple HO wave function in the theoretical calculation. Therefore, the internal energy of the  $^5\text{He}$  wave function is higher than the realistic  $^5\text{He}$  nucleus.

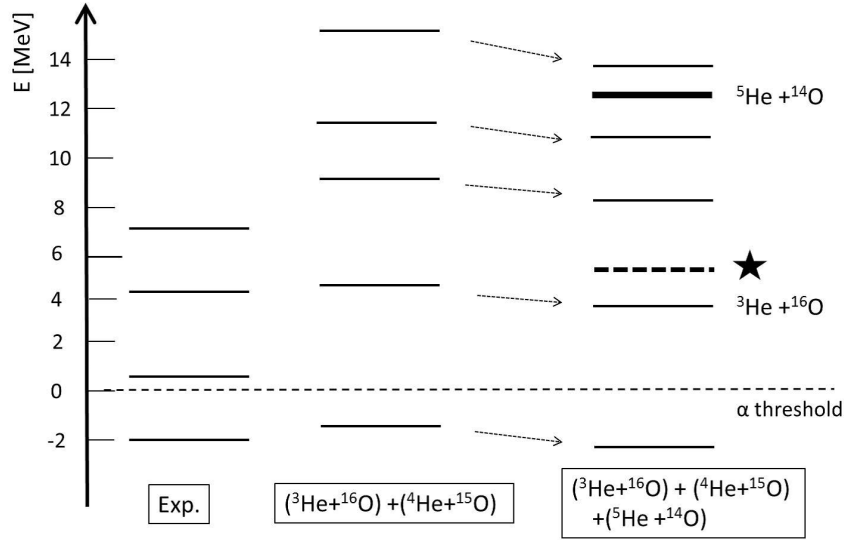


**Figure 2:** Energy spectra for the  $3/2^+$  state. The left levels shows the experimental spectra of the  $3/2^+$  state, while the middle and right spectra are the results of the microscopic calculation. The middle levels are the GCM solution of  $(^3\text{He}+^{16}\text{O}) + (\alpha+^{16}\text{O})$ , while the right levels are the result of the  $(^3\text{He}+^{16}\text{O}) + (\alpha+^{16}\text{O}) + (^5\text{He}+^{14}\text{O})$  calculation. The arrows indicate the corresponding levels between the middle levels and the right levels. This figure is taken from Ref. [13]. See text for details.

Let us discuss the energy shift, which will arise from the correction of the threshold energy. If the  $^5\text{He} + ^{14}\text{O}$  threshold is correctly reproduced, the energy of  $^5\text{He} + ^{14}\text{O}$  will simply shift to the lower energy region by about 7 MeV, as shown by the dashed level with the star at the right level. Other levels will be unchanged even if the shift of the  $^5\text{He} + ^{14}\text{O}$  level occurs. This is because of the de-coupling feature of  $^5\text{He} + ^{14}\text{O}$  from the model space of the  $(^3\text{He}+^{16}\text{O}) + (\alpha+^{15}\text{O})$  coupled-channels. Therefore, the excitation energy of  $^5\text{He}+^{14}\text{O}$  will be simply changed into  $E_x \sim 5$  MeV with respect to the  $\alpha$  threshold, (dashed level with the star). In this situation, the level repulsion is possible between the corrected  $^5\text{He} + ^{14}\text{O}$  state and the level at  $E_x \sim 4$  MeV, which has a main component of  $^3\text{He} + ^{16}\text{O}$ . Since the matrix element of the two neutron transfer is evaluated to be about 1  $\sim$  2 MeV, the energy shift of the  $^3\text{He} + ^{16}\text{O}$  state, which is generated from the perturbative coupling with  $^5\text{He} + ^{14}\text{O}$  level, is estimated to be about  $-3$  MeV. Therefore, there is a possibility that the  $3/2^+$  state appear around the  $\alpha$  threshold within the energy rang of about 1  $\sim$  2 MeV if the theoretical  $^5\text{He}$  threshold is reproduced correctly.

In order to confirm the conjecture about the level shift of the  $^5\text{He} + ^{14}\text{O}$  state, we perform the modified GCM calculation, in which the threshold energies are corrected by the phenomenological manner. The matrix element of the total Hamiltonian  $H$  can be decomposed into the internal and relative parts in the case of the diagonal transition, such as

$$H_{\alpha,\alpha}(S',S) = H_{\alpha,\alpha}^{(rel)}(S',S) + H_{\alpha,\alpha}^{(in)}(S',S) \quad (3.1)$$

with the definition of

$$O_{\alpha,\alpha}(S',S) = \langle \Phi_{\alpha}^{J\pi}(S') | \hat{O} | \Phi_{\alpha}^{J\pi}(S) \rangle, \quad (3.2)$$

where  $H_{\alpha,\alpha}^{(rel)}$  and  $H_{\alpha,\alpha}^{(in)}$  denote the relative and internal parts of the diagonal matrix elements with the channel bases of  $\Phi_{\alpha}^{J^{\pi}}(S)$ . Here, the channel basis are constructed from a specific linear combination of the AO basis,  $\Phi_{\mathbf{m}}^{JK}(S)$ , given in Eq. (2.1). If the internal wave functions of He and O are in the exact eigenstate of the internal Hamiltonian,  $H_{\alpha,\alpha}^{(in)}(S', S_{\alpha})$  holds the following relation

$$H_{\alpha,\alpha}^{(in)}(S', S) = E_{\alpha}^{(in)} N_{\alpha,\alpha}(S', S) , \quad (3.3)$$

where  $E_{\alpha}^{(in)}$  and  $N_{\alpha,\alpha}(S', S)$  represent the internal energy and the overlap matrix element ( $\hat{O} = 1$ ) in the channel  $\alpha$ . Since the overlap matrix of  $N_{\alpha,\alpha}(S', S)$  goes to unity in the asymptotic limit of  $S = S' \rightarrow \infty$ ,  $E^{(in)\alpha}$  determines the dissociation energy of  $^{19}\text{Ne}$  into two fragments of He + O in the channel  $\alpha$ .

In order to correct the threshold energies, we modify the Hamiltonian matrix elements for the transition of  $\alpha \rightarrow \beta$  according to the following replacement,

$$H_{\beta,\alpha}(S_{\beta}, S_{\alpha}) \rightarrow H_{\beta,\alpha}(S_{\beta}, S_{\alpha}) + \Delta E_{\alpha} \cdot N_{\beta,\alpha}(S_{\beta}, S_{\alpha}) \delta_{\alpha,\beta} . \quad (3.4)$$

Here,  $\Delta E_{\alpha}$  means the energy correction to reproduce the threshold of the channel  $\alpha$  correctly. According to Eq. (3.4), we set the threshold energy of the  $^3\text{He} + ^{16}\text{O}$  and  $^5\text{He} + ^{14}\text{O}$  to 8.4 and 14 MeV, respectively, which are experimental energy. In the modified GCM calculation, we have found that the  $3/2^+$  resonance appears around  $E \sim 2$  MeV with respect to the  $\alpha$  threshold. Therefore, the correction of the threshold energy leads to decreasing the excitation energy of the  $^5\text{He} + ^{14}\text{O}$  state, which originally exists at  $E \sim 12$  MeV in Fig. 2.

#### 4. Summary and discussion

We have applied the microscopic cluster model, generalized two-center cluster model (GTCM), to the  $^{19}\text{Ne}$  nucleus, and the energy levels are discussed. In GTCM, the basis functions are constructed from the possible partitions of the valence neutrons around the  $^3\text{He}$  and  $^{14}\text{O}$  cores, and the anti-symmetrization among all the nucleons is completely taken into account. This model can produce the smooth connection of the weak coupling states and the strong coupling states in the adiabatic energy curves, which are the series of the energy eigenvalues as a function of the core distance. The GTCM calculation nicely reproduces the bound low-lying levels and predicts the possible appearance of the highly resonant levels. The experimental identification of the highly resonances is strongly desired.

However, the present calculations do not reproduce the  $3/2^+$  and some levels in the vicinity of the  $\alpha$  threshold. The threshold  $3/2^+$  resonance is considered to have the main component of the  $5p-2h$  shell model configuration [15]. The  $5p-2h$  configuration corresponds to the  $^5\text{He} + ^{14}\text{O}$  configuration in the shell model limit and hence, we have performed the extended calculation, which takes into account the  $^5\text{He} + ^{14}\text{O}$  configuration. The extended calculation suggests the formation of a new  $3/2^+$  state, which has the dominant component of the  $^5\text{He} + ^{14}\text{O}$  channel, but its excitation energy is much higher than the experimental data. To improve the shortcomings of the calculation, we have corrected the threshold energies in a phenomenological manner. In the modified calculation, we have confirmed a new  $3/2^+$  state appear around  $E \sim 2$  MeV with respect to the  $\alpha$  threshold.

The phenomenological correction of the threshold energy, which is employed in the preset analysis, is not correct prescription but the approximated treatment. In the correct treatment, the off-diagonal matrix elements should also be modified in connection to the replacement of the diagonal elements in Eq. (3.4). Since the exact treatment of all the threshold energies will be quite difficult in the microscopic approach, the threshold energy should be handled in a phenomenological manner. In order to overcome this threshold problem, the semi-microscopic cluster model, the orthogonalized condition model (OCM) [10], is considered to be better approach than the full microscopic approach. In the OCM calculation, the threshold energies of all the open channels are handled in a phenomenological manner, in which the theoretical threshold energies to be set to the experimental value. Thus, the application of the OCM calculation will be effective to solve the problem the  $3/2^+$  state just above the  $\alpha$  threshold. The semi-microscopic OCM calculation is now under progress.

## References

- [1] K. Ikeda et al., Prog. Theor. Phys. Suppl. **68**, 1 (1986).
- [2] H. Horiuchi et al., Suppl. Prog. Theor. Phys. **192**, 1 (2012), and references therein.
- [3] M. Freer, Rep. Prog. Phys. **70**, 2149 (2007).
- [4] M. Ito and K. Ikeda, Rep. Prog. Phys. **77**, 096301 (2014).
- [5] N. Itagaki, T. Otsuka, K. Ikeda and S. Okabe, Phys. Rev. Lett. **92**, 142501 (2004).
- [6] Masaaki Kimura, Phys. Rev. **C75**, 034312 (2007).
- [7] T. Yamada and Y. Funaki, Phys. Rev. **C82**, 064315 (2010).
- [8] B. Buck and A. A. Pilt, Nucl. Phys. **A280**, 133 (1977).
- [9] F. Nemoto and H. Bando, Prog. Theor. Phys. **47**, 1210 (1972).
- [10] T. Sakuda and F. Nemoto, Prog. Theor. Phys. **62**, 1274 (1979).
- [11] P. Descouvemont and D. Baye, Nucl. Phys. **A463**, 629, (1986).
- [12] R. Otani et al., Phys. Rev. **C90**, 034306 (2014).
- [13] R. Otani, M. Iwasaki and M. Ito, EPJ Web of Conferences **122**, 11003 (2016).
- [14] K. Langanke et al., Astrophys. Jour. **301**, 629 (1986).
- [15] Z. Q. Mao et al., Phys. Rev. Lett. **74**, 3760 (1995).
- [16] H. Horiuchi, Suppl. Prog. Theor. Phys. **62**, 90 (1977).
- [17] A. B. Volkov, Nucl. Phys. **74**, 33 (1965).
- [18] N. Yamaguchi, T. Kasahara, S. Nagata, and Y. Akaishi, Prog. Theor. Phys. **62**, 1018 (1979).
- [19] Andra T. Kruppa, and K. Kato, Prog. Theor. Phys. **84**, 1145 (1990).
- [20] Y. Takenaka et al., Prog. Exp. Theor. **2014**, 113D04 (2014).
- [21] H. Yamaguchi et al., Phys. Rev. **C87**, 034303 (2013); H. Yamaguchi et al., Phys. Rev. **C83**, 034306 (2011).